Int. J. Multiphase Flow Vol. 16, No. 4, pp. 727–740, 1990
Printed in Great Britain.

0301-9322/90 $3.00 + 0.00

MEASUREMENTS OF DOUBLE-LAYER REPULSION FOR SLIGHTLY OVERLAPPING COUNTERION CLOUDS

S. G. BIKE† and D. C. PRIEVE
Department of Chemical Engineering, Carnegie Mellon University, Pittsburgh, PA 15213, U.S.A.

(*Received* 4 *June* 1989; *in revised form* 15 *February* 1990)

Abstract—Total internal reflection microscopy (TIRM) has recently been developed as a new technique to measure directly the mean potential energy of interaction between a single colloidal particle and a flat plate. TIRM provides instantaneous measurements of the relative separation between the particle and the plate, which are derived from the intensity of light scattered by the particle from the evanescent wave established upon total internal reflection at the plate/liquid interface. Using Boltzmann's equation, potential energy profiles are then obtained from histograms or relative separation distance. We have used TIRM to obtain (noninvasively) intensity distributions for a single 10 μm polystyrene sphere located near a flat glass plate in a series of electrolyte solutions. Potential energy diagrams derived from the scattering histograms compare very well with those expected based on simple models of double-layer and gravity forces which involve no adjustable parameters. These potential energy profiles have confirmed the exponential decay of double-layer repulsion with the Debye length as the decay length. The experimental methods have been refined to permit smaller background ionic strengths and longer sampling times. The spatial resolution of TIRM is shown to be on the order of nanometers.

Key words: double-layer repulsion, colloidal forces, total internal reflection, light scattering, evanescent wave

INTRODUCTION

A new technique, total internal reflection microscopy (TIRM), has recently been developed which provides accurate and instantaneous measurements of relative separation distances (relative to the most probable) between a single microscopic particle and a flat surface (Prieve *et al.* 1987; Bike 1988). Using Boltzmann's equation, potential energy profiles can then be derived from histograms of these distance measurements. Consequently, with TIRM we can directly measure the mean potential of the interaction force between a microscopic particle and a flat surface. While direct force measurements have been made between macroscopic bodies with the crossed-mica cylinder technique (Israelachvili & Adams 1976, 1978), such measurements have yet to be realized using two colloidal particles; the primary obstacles to achieving these measurements include the small size of the particles and the small magnitude of the interaction forces. TIRM thus presents a compromise between force measurements using two macroscopic surfaces and force measurements using two colloidal particles.‡

TIRM is based on the total internal reflection of light at an interface separating two media of different refractive indices. When total internal reflection occurs, an evanescent electromagnetic wave penetrates into the less optically dense medium. Any material of unmatched refractive index located in this wave will scatter light at an intensity which decays exponentially with the normal distance from the interface. Consequently, measurements of the scattered light intensity give an exponentially-sensitive measure of the distance at which the scatter is located from the interface.

We have used this phenomenon to observe noninvasively the dynamics of a single colloidal particle in close proximity to a flat surface. We deduced relative separation distances between a single Brownian sphere and a glass plate (reflecting interface) from measurements of the scattered light intensity in a series of electrolyte solutions. Potential energy diagrams then were constructed based on histograms of the scattered light intensity. Not only did these diagrams demonstrate the influence of both double-layer repulsion and gravity on the sphere's movement, but they also agreed

†Present address: Department of Chemical Engineering, University of Michigan, Ann Arbor, MI 48109-2136, U.S.A.
‡Note that while the crossed-mica cylinder technique provides the potential of the mean interaction force, TIRM provides the mean potential of the force.

very well with those predicted from models of these forces. The agreement obtained at larger relative separation distances, for which the potential energy curve is linear with a slope equal to the known force of gravity, provided the strongest confirmation of the ability of TIRM to measure colloidal forces. In addition, these potential energy diagrams have confirmed the exponential decay of double-layer repulsion with the Debye length as the decay length. With regard to the earlier experiments with TIRM (Prieve *et al.* 1987), the experimental methods have now been refined to permit smaller background ionic strengths and longer sampling times.

The resolution achieved with this technique is on the order of nanometers, comparable to scanning electron microscopy (SEM); unlike SEM, however TIRM can be used to study particle dynamics in liquid media. This work has demonstrated the potential of TIRM to measure other colloidal forces, including van der Waals and steric forces, and additionally to quantify particle adsorption/desorption processes in either quiescent or moving fluids.

In this paper, the principles of total internal reflection are first reviewed, followed by a description of our experimental technique incorporating this phenomenon to measure colloidal forces. The experimental results are next presented and compared with the predictions of the force models. Finally, future applications of TIRM are outlined.

BACKGROUND

Techniques to Measure Colloidal Forces

One well-known technique to measure colloidal forces is the crossed-mica cylinder technique developed by Israelachvili & Adams (1976, 1978). Atomically smooth mica sheets are glued onto macroscopic polished glass cylinders (radius of curvature ≈ 1 cm) which are placed at right angles. The cylinders are then pushed together by a known force, and the separation distance between the cylinders at equilibrium is measured by interferometry. Separation distances down to contact can be measured with an accuracy of ± 0.1 nm. Applications of this technique include the measurement of van der Waals and double-layer forces (Israelachvili & Adams 1976, 1978; Israelachvili 1978), solvation forces (Christenson *et al.* 1982; Christenson & Horn 1983; Christenson 1984) and steric forces (Israelachvili *et al.* 1980; Israelachvili 1984). Another force-measuring technique has been developed by Rabinovich *et al.* (e.g. Rabinovich *et al.* 1982) which uses crossed-quartz filaments of radii on the order of millimeters. Note that both of these techniques measure the potential of the mean interaction force. Colloidal particles, unlike the macroscopic bodies, experience a random Brownian force. Although the time average of this Brownian force vanishes, the existence of this force can make the potential of the mean force different from the mean potential.

While these techniques using macroscopic bodies have been successful, it is difficult to measure directly the interaction forces between individual colloidal particles for two reasons. First, the small size of colloidal particles (on the order of 1 nm to 1 μm) prohibits one from simply pushing two particles together with a known force and measuring the distance between them at equilibrium. Second, the small magnitude of interaction forces (typically $\leqslant 10^{-7}$ dyn) makes these forces difficult to measure directly.

Prieve & Alexander (1986; Alexander & Prieve 1987) have developed a hydrodynamic technique to measure the mean potential energy of interaction between a single colloidal particle and a flat plate. Sphere/wall separation distances are determined from measurements of particle speed during slow linear shear flow of the dispersing fluid. Potential energies inferred from histograms of these distances have demonstrated the presence of double-layer repulsion. While the spatial resolution of this hydrodynamic technique is two orders of magnitude less than that of the crossed-mica cylinder technique, it does have the advantages of reducing one surface to colloidal dimensions and of measuring very small forces. However, this technique cannot provide measurements of separation distance in real-time, and the conversion of the speed measurements to separation distances is time consuming. In addition, Prieve & Alexander (1986) observed an unexpected migration of the particle away from the wall during the development of this technique; Prieve & Bike (1987; Bike & Prieve 1990) later ascribed this migration to a newly-recognized colloidal force called electrokinetic lift.

The philosophy of the hydrodynamic technique—monitoring the Brownian fluctuations of a colloidal particle that is interacting with a flat plate—has formed the basis of a new technique to measure colloidal forces called total internal reflection microscopy (TIRM) (Prieve *et al.* 1987; Bike 1988). While changes in separation distance are detected through changes in particle speed with the hydrodynamic technique, changes in separation distance are detected through changes in scattered light intensity with TIRM. As a result, TIRM, unlike the hydrodynamic technique, can also be applied to quiescent systems and has a much greater spatial resolution (comparable to SEM). Similar to the hydrodynamic technique, TIRM is a noninvasive technique that can be used to study particle dynamics in liquid media.

Principles of TIRM

When light encounters an interface between two transparent media of different refractive indices n_i, the light is partially reflected and partially transmitted (figure 1). From Maxwell's equations, refraction of the transmitted beam is described by Snell's law (Lipson & Lipson 1981):

$$\sin\theta = n_{21}\sin\theta', \qquad \text{where } n_{21} \equiv \frac{n_2}{n_1}, \qquad [1, 2]$$

θ is the angle of incidence and θ' is the angle of refraction. If the light approaches the interface from medium 1 and $n_1 > n_2$, reflection of the light is called internal reflection. Note that as θ increases, θ' must also increase. When $\theta' = 90°$, θ corresponds to the critical angle θ_c,

$$\theta_c = \sin^{-1} n_{21}. \qquad [3]$$

For incident angles $\theta > \theta_c$, θ' is imaginary and the light beam is totally reflected at the interface. This phenomenon is called *total internal reflection*. While no net energy is transmitted into the less-optically-dense medium 2, an evanescent electromagnetic wave does penetrate a short distance from the interface into this medium. The intensity I_{ev} of the evanescent wave, which is proportional to the square of the electric field magnitude, decays exponentially with the normal distance z from the interface (Lipson & Lipson 1981):

$$I_{ev} = I_{ev,0}\exp\left(\frac{-z}{d_p}\right); \qquad [4]$$

$I_{ev,0}$ is the evanescent electric field intensity at the interface ($z = 0$) and d_p is the characteristic penetration depth of the wave,

$$d_p = \frac{\dfrac{\lambda_0}{n_1}}{4\pi(\sin^2\theta - n_{21}^2)^{1/2}} \qquad [5]$$

where λ_0 is the wavelength of the light. d_p, which is independent of the incident beam polarization, increases both as θ approaches θ_c and as n_{21} approaches 1, and is on the order of the wavelength of the incident light except for θ close to θ_c.

When located near the reflecting interface, light scatterers, light absorbers or any material of refractive index $n_3 \neq n_2$ will scatter radiation from the evanescent wave. The phenomenon of total internal reflection is commonly applied to the study of fluorescently-tagged molecules or particles either bound to or in the near vicinity of an interface; this application is known as total internal reflection fluorescence (TIRF) (Axelrod *et al.* 1984). Previous uses of TIRF include the study of cells grown on glass substrates (Lanni *et al.* 1985), the characterization of protein adsorption kinetics at the solid/liquid interface (Watkins & Robertson 1977; Beissinger & Leonard 1980) and the observation of interfacial depletion layers between polymer solutions and a solid wall (Allain *et al.* 1982; Ausserre *et al.* 1985). In addition, Lan *et al.* (1986) have studied the dynamic behavior of Brownian particle ensembles near a wall using photon correlation to analyze the scattering from an evanescent wave. Surface defects can also give rise to scattering from the evanescent wave: the acronym "TIRM" was first used to describe a qualitative surface inspection technique for identifying sites of surface irregularities or inclusions (Temple 1981).

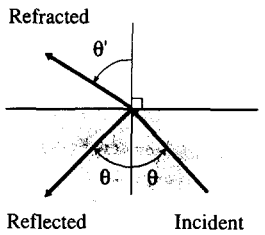

Figure 1. Internal reflection.

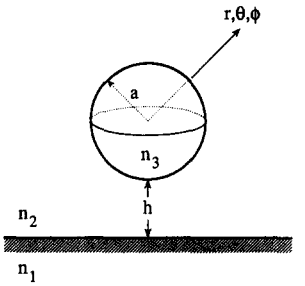

Figure 2. Geometry for a dielectric sphere scattering in the evanescent wave in the vicinity of a planar wall.

Chew *et al.* (1979) have developed a theory for the elastic scattering of evanescent waves by dielectric spheres. Defining the sphere as medium 3 (figure 2), the expression for the scattered field $\mathbf{E}_{sc}$ is given by

$$\mathbf{E}_{sc}(r, \theta, \phi) = A \exp\left(\frac{-h}{2d_p}\right) \sum_{l,m} \mathbf{B}_{l,m}(\theta, \phi) \qquad \text{for large } r, \qquad [6]$$

where

$$A = \frac{\exp(ik_2 r)}{k_2 r}, \qquad [7]$$

k_2 is the wavenumber in medium 2 and h is the sphere–plate separation distance. Equation [6] assumes that multiple reflections between the sphere and the reflecting interface can be neglected. The vectors $\mathbf{B}_{l,m}$ involve both spherical harmonics and expansion coefficients. The spherical harmonics are functions of the angles θ and ϕ at which the scattering is observed. The expansion coefficients depend on the particle radius a and on the refractive indices and dielectric constants in media 2 and 3; however, the coefficients are independent of the separation distance h. As a result, the intensity of the scattered light, which is proportional to the square of the magnitude of $\mathbf{E}_{sc}$, simply decays exponentially with the normal distance from the reflecting interface:

$$I(h, \Omega) = I(0, \Omega)\exp\left(\frac{-h}{d_p}\right), \qquad [8]$$

where $I(h, \Omega)$ is the integral of the scattered light intensity over a solid angle Ω corresponding to the numerical aperture of the objective. Consequently, measurements of the scattering intensity provide an exponentially-sensitive measure of the separation distance. Note that the region over which the evanescent wave is operative can be "fine-tuned" by adjusting d_p through changes in the incident angle, [5]; it is thus possible to study phenomena very near to the interface by selecting θ near to 90° or very far from the interface by selecting θ near to θ_c.

For the experiments described in this paper, only separation distances relative to the most probable (i.e. relative to the separation distance at the most-frequently observed scattering intensity) are reported. Measurements of the absolute separation distance require knowledge of $I(0, \Omega)$. In principle $I(0, \Omega)$ can be determined by measuring the scattering intensity from a particle adsorbed onto the reflecting interface. However, [8] assumes that the particle is located sufficiently far from the interface such that multiple reflections can be neglected; an absorbed particle violates this assumption, and we would then expect the functional form of [8] to be altered. Approaches to determining absolute separation distances are discussed at the end of this paper.

Preliminary Work with TIRM

Prieve *et al.* (1987) pursued the initial development of TIRM as a technique to measure separation distances between a colloidal particle and a flat plate. Brownian fluctuations in separation distance between a single 10 μm polystyrene latex microsphere and a glass slide were detected through changes in the scattered light intensity. Potential energy diagrams derived from the scattering measurements revealed the action of double-layer repulsion which was weakened by the addition of salt. While these experimentally-derived potential energy diagrams

were qualitatively similar to those predicted from models of double-layer and gravity forces, the diagrams were quantitatively different from those predicted; this difference was most pronounced at high ionic strengths (smaller sphere/plate separation distances). They suggested that van der Waals attraction, which was not accounted for in their predictions, was one possible cause of the discrepancy. Note that Prieve *et al.* (1987) used sodium dodecyl sulfate (SDS) as the surfactant in the dispersions and, consequently, were constrained to high background ionic strengths contributed by the SDS. As a result, only a limited range of ionic strengths, and correspondingly separation distances, were studied.

In addition, sampling times were limited to 10 min to minimize changes in the ionic strength during an experiment due to evaporation of the solution. While an infinite amount of time is required for a particle to sample all separation distances represented in the probability distribution, given a very long (but finite) time the particle will sample enough separation distances represented in the central portion of the distribution to allow the shape of the distribution to converge ("equilibrium" histogram). It is likely that their scattering histograms may not have represented equilibrium histograms because of the short observation times. Note that we have now refined the experimental techniques to permit smaller background ionic strengths and longer sampling times.

EXPERIMENTAL

Apparatus

Two different light sources were used in these TIRM experiments: (1) a 5 mW HeNe laser ($\lambda_0 = 632.8$ nm; Melles Griot); and (2) a 50 mW tunable Ar ion laser ($\lambda_0 = 454$–514.4 nm; Omnichrome). Both lasers are linearly polarized at 500:1. As depicted in figure 3(a), the laser beam is directed to a first-surface Al mirror mounted on a rotating stage with a micrometer mount for positioning (Klinger Scientific), which allowed precise control of the incident angle. The rotating stage is mounted on an optical rail, allowing translation of the mirror parallel to the laser beam; this translation is necessary when the angle of incidence is changed. Reflecting from the mirror, the light is then directed to a cubic prism constructed of BK-7 glass ($n = 1.520$ at $\lambda = 514.4$ nm and 1.515 at $\lambda = 632.8$ nm).

The experimental system studied consisted of a 10 μm polystyrene microsphere interacting with a glass microscope slide in a series of electrolyte solutions [figure 3(b)]. A sample of a dilute dispersion of the particles was placed in a glass well approx. 2 cm dia and 0.7 cm high fused to a glass microscope slide. This slide was optically coupled to the upper face of the prism with immersion oil ($n = 1.518$ at 23°C), with total internal reflection occurring at the glass/water interface. The light scattered by one particle was measured using a Zeiss photometry system incorporating a Hamamatsu photomultiplier tube (PMT) and a Zeiss photomultiplier readout device sampled at a known rate by an A/D board (Keithley) which was interfaced with an IBM PC/AT.

The HeNe laser was used to verify that TIRM could be used to measure separation distances. With this laser, however, the intensity of light scattered by a particle at the smaller ionic strengths

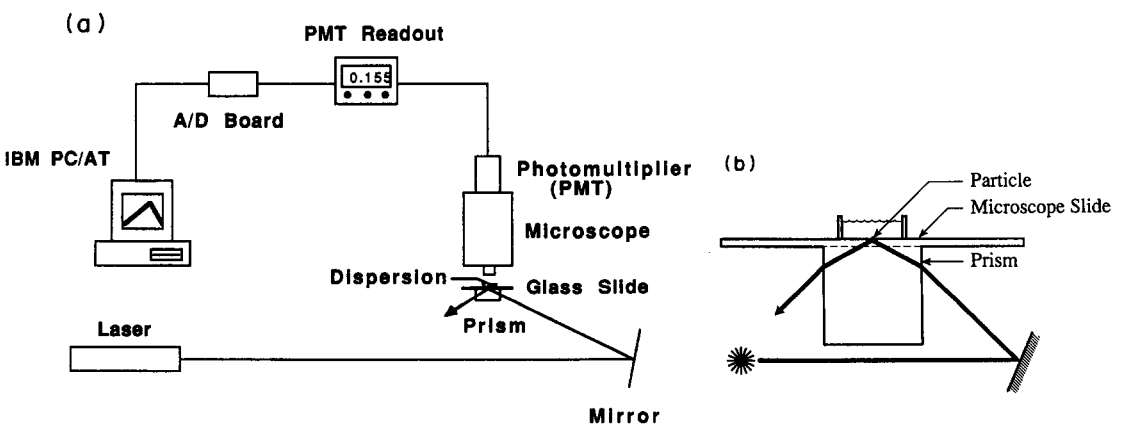

Figure 3. (a) Schematic of the experimental setup for the TIRM experiments. (b) Expanded view of a colloidal sphere interacting with the microscope slide optically coupled to the prism.

Table 1. Physical properties of the solutions

mM NaCl added (approximate)	0	0.1	0.3	1.0	3.0	10.0
Conductivity[a] ($\mu\Omega^{-1}\,cm^{-1}$)	3.75	22.5	49.7	128	378	1260
Ionic strength (mM) (calculated)	0.030	0.178	0.303	1.01	2.99	9.96
Debye length (nm)	55.6	22.8	15.4	9.57	5.56	3.04

[a]Measured at 25°C.

was near the limit of detection of the PMT because the particle was located in the lower-intensity "tail" of the evanescent wave. As a result, the more powerful 50 mW Ar ion laser was incorporated into the design. Not only can the intensity of the laser light be manually controlled with this Ar ion laser, but also the wavelength of the laser light can be tuned to one of nine wavelengths.

Materials

The colloidal particles selected for these experiments were polystyrene latex microspheres of dia $9.87 \pm 0.06\ \mu m$ (Duke Scientific). The relatively large size of these particles gave rise to a significant scattered light intensity, so that light scattered by a single particle was easily detected by the PMT. In addition, the large size resulted in a substantial gravity force acting to push the particles toward the surface of the glass slide and thus into the evanescent wave. The low standard deviation in the particle size alleviated variations in the scattered light intensity between different particles within the same sample due to variations in the particle size, and also eliminated the difficult task of measuring the size of each particle.

The dispersion media (table 1) were prepared by diluting a filtered 1 M NaCl (Fisher Scientific A.C.S. grade) stock solution with filtered deionized water containing 0.75 mM octaethyleneglycol mono n-decyl (Nikko Chemical Co. Ltd). The nonionic surfactant was added to discourage sticking of the particles to the glass slide, which was more prevalent at higher ionic strengths. Additionally, the use of a nonionic removed the limitation of high background ionic strength experienced by Prieve *et al.* (1987) with SDS.

Procedure

Immediately prior to an experiment, one drop of the particle stock dispersion as received (0.3% vol concentration) was added to 100 ml of a selected dispersion medium. Approximately $2\ cm^3$ of the resulting particle dispersion was placed in the well on the microscope slide coupled to the prism [figure 3(b)]. A 40 × water-immersion lens was carefully submerged into the dispersion; the exposed liquid surface was covered with Parafilm® to prevent evaporation and any associated change in ionic strength of the solution. This procedural change from Prieve *et al.* (1987) allowed us to achieve much longer sampling times (at least 20 min) and thus to approach more closely the equilibrium histogram of separation distances.

Using two translating stages, the prism was moved laterally and longitudinally until one particle well-separated from other particles was located in the field of view of the microscope. A rectangular aperture in the photometer of the microscope was then adjusted so that only this one particle would be "seen" by the PMT; typically, the aperture was 3 particle diameters square and the dimensions of the aperture were not changed during an experiment so as to maintain a constant background intensity. With the laser on, the angle of the mirror was adjusted to give a maximum reading of the scattered light intensity on the PMT readout. Since the intensity distribution across the incident beam is Gaussian, the maximum in the PMT readout corresponds to the particle being centered within the incident beam.

When one particle was located and the mirror positioned accordingly, the room was darkened and the scattered light intensity recorded for 2 min. This preliminary check of the scattered light intensity served to discriminate between "stuck" and "free" particles; the scattered light intensity from a "stuck" particle was of higher magnitude and varied over a smaller range (as a percent of the mean) than the scattered light intensity from a "free" particle. Only "free" particles were selected for experimentation.

Once a particle was determined to be "free" the digital signal from the PMT was sampled every 30 ms by the A/D board for at least 20 min to ensure that the histogram converged to represent an equilibrium sampling of separation distances. The shape of the histogram converged in <4 min at the lowest ionic strength, but did not converge until approx. 16 min at the highest ionic strength.† Every 1–2 min, the data collection was halted, and the position of the particle was checked with respect to the axis of the microscope. If the particle had left the window seen by the PMT, the data from that particular time segment was discarded. If necessary, the particle was repositioned within the window; repositioning was more common at the lower ionic strengths, as the particle experienced a higher mobility due to the larger particle/slide separation distance.

While it is desirable that the PMT "see" only light scattered by the sphere, it was not possible to isolate the equipment from external light. Consequently, the background intensity without a particle present in the field of view was also recorded and then subtracted from the measured scattered light intensity to give the intensity of light scattered by the sphere alone. The background intensity, which varied primarily with the light conditions outside, is independent of ionic strength; as a result, this intensity was more important in the lower ionic strength solutions for which the scattered light intensity was lower (due to the greater particle–wall separation distance). For example, the background intensity represented approx. 10% of the scattering intensity for a particle in the 0 mM solution but $<1\%$ for a particle in the 10 mM solution.

Data Analysis

Histograms of scattered light intensity

Using a combination of Keithley-supplied and user-written programs, the data collected in each 1–2 min interval was converted into a histogram of frequency vs scattering intensity relative to the background intensity. This intensity was assumed to be linearly proportional to the voltage signal from the PMT (this assumption is justified by the agreement of the data with the theory, as shown in the next section). Each histogram was reviewed, and histograms in which the particle became stuck or in which the particle left the aperture window were discarded. For each particle, all acceptable individual histograms were then added together to form the total histogram, which was condensed by combining 5, 10 or 20 neighboring intervals of intensity into one interval to smooth the shape of the histogram. The larger the range of measured scattering intensities, the greater the number of intervals that were condensed into one interval.

Experimental potential energy diagrams

Experimental potential energy profiles were deduced from each total histogram according to the analysis of Prieve *et al.* (1987). Denoting the separation distance corresponding to the most-probable intensity as h_2, the most-probable intensity and the frequency of this intensity are given as $I(h_2)$ and $N(h_2)$, respectively. Separation distances between the sphere and the plate are found from the scattering intensities using [8]; dividing both sides of this equation at a given h by the same equation at h_2 gives

$$h - h_2 = d_p \ln\left[\frac{I(h_2)}{I(h)}\right]. \qquad [9]$$

When the observation time of the scattering becomes arbitrarily large, the shape of the histogram of frequency vs intensity approaches the shape of the probability density function for the intensity, $P(I)$. The probability $p(h)\mathrm{d}h$ of locating a particle at a separation distance between h and $h + \mathrm{d}h$ is the same as the probability $p(I)\mathrm{d}I$ of observing a scattering intensity between I and $I + \mathrm{d}I$,

$$p(h) = P(I)\frac{\mathrm{d}I}{\mathrm{d}h}, \qquad [10]$$

which gives‡

$$\frac{\mathrm{d}p}{\mathrm{d}h} = \frac{\mathrm{d}P}{\mathrm{d}I}\left(\frac{\mathrm{d}I}{\mathrm{d}h}\right)^2 + P\frac{\mathrm{d}^2I}{\mathrm{d}h^2}. \qquad [11]$$

†The tails of the histograms never fully converge due to the infrequent sampling of the corresponding high-energy states.
‡Note that the separation distance h_m at which $\mathrm{d}p/\mathrm{d}h = 0$ (discussed in the next section) does not necessarily correspond to the separation distance h_2 at which $\mathrm{d}P/\mathrm{d}I = 0$.

Differentiating [8] with respect to h gives

$$\frac{dI}{dh} = \frac{-I}{d_p}. \quad [12]$$

Substituting this result into [10] yields the probability of locating a particle at h relative to the corresponding probability at h_2:

$$\frac{p(h)}{p(h_2)} = \frac{P[I(h)]I(h)}{P[I(h_2)]I(h_2)}. \quad [13]$$

Assuming that $p(h)$ is described by a Boltzmann distribution,

$$\frac{p(h)}{p(h_2)} = \exp\left[\frac{V(h) - V(h_2)}{kT}\right], \quad [14]$$

[13] can be transformed into a relationship between the potential energy $V(h)$ at h relative to that at h_2 and the scattering intensity and frequency:

$$\frac{V(h) - V(h_2)}{kT} = \ln\left[\frac{N[I(h)]I(h)}{N[I(h_2)]I(h_2)}\right], \quad [15]$$

where the frequency $N(I)$ has replaced $P(I)$.

Predicted potential energy profiles

Additionally, the shape of the potential energy diagram can be predicted from models for the forces present in the sphere/plate system. Assuming that only gravity and double-layer forces are important in determining the separation distance between the sphere and the plate, the total potential is written as

$$V(h) = V_R(h) + V_g(h), \quad [16]$$

where

$$V_R(h) = B \exp(-\kappa h), \quad [17]$$

$$B = 16\, a\varepsilon\left(\frac{kT}{ze}\right)^2 \tanh\left(\frac{ze\zeta_1}{4kT}\right)\tanh\left(\frac{ze\zeta_2}{4kT}\right), \quad [18]$$

$$V_g(h) = Gh \quad [19]$$

and

$$G = \tfrac{4}{3}\pi a^3 g \Delta\rho \quad [20]$$

where $V_R(h)$ and $V_g(h)$ are the double-layer and gravity potentials, respectively, ε is the dielectric constant of the fluid, k is Boltzmann's constant, T is the absolute temperature, z is the charge number (assuming a symmetric electrolyte), e is the protonic charge, ζ_i is the potential of surface i, κ is the inverse Debye length, g is the gravitational acceleration and $\Delta\rho$ is the density difference between the fluid and the particle. The minimum in total potential occurs at the separation distance h_m, where

$$h_m = \kappa^{-1} \ln\left(\frac{\kappa B}{G}\right). \quad [21]$$

The form of the double-layer potential given above is neither based on the linearized Poisson–Boltzmann equation nor assumes constant surface potential. Instead, [17] and [18] are obtained by superimposing the electrostatic potential profile (derived from the nonlinear Poisson–Boltzmann equation for a symmetric binary electrolyte) for two isolated plane double layers and then applying Derjaguin's approximation to calculate the interaction between two spheres. Consequently, the given form of the double-layer repulsion requires only that $\kappa a \gg \kappa h \gg 1$.

Using [21], the parameter B can be eliminated from the expression for the total potential; this elimination is fortunate since the parameter B contains information that at present has not been

determined independently (i.e. the zeta potentials). The potential at h referenced to that at h_m is then given by

$$\frac{V(h) - V(h_m)}{kT} = \frac{G}{kT}\left\{\frac{\exp[-\kappa(h - h_m)] - 1}{\kappa} + (h - h_m)\right\}. \quad [22]$$

Equation [22] predicts a linear region in the potential energy at large $h - h_m$: at these separation distances, only gravity should act on the sphere, and the gravitational potential is linear in h, [19]. This predicted potential energy profile can then be compared with the deduced experimental potential energy profile, [15].

No adjustable parameters are required to construct the predicted potential energy profile. The only unknown parameter in [22] is the inverse Debye length κ; however, this parameter is a function of the ionic strength of the solution which can be calculated from the measured solution conductivity. For the solutions employed in our experiments, the conductivity was converted to ionic strength using the limiting ionic conductances of H^+, Na^+ and Cl^- ions, assuming that other ionic species that might have been present contributed insignificantly to the conductivity.

RESULTS AND DISCUSSION

Changing Ionic Strength

Histograms of scattered light intensity

Histograms of scattering intensity for one sphere each in a solution of ionic strength from 0 to 3 mM are shown in figure 4. These data were obtained with the 5 mW HeNe laser. Frequency, $N(I)$, represents the number of times that a scattering intensity in the interval $(I - \Delta I,\ I + \Delta I)$ was observed. Note that the peak maxima are displaced to a higher relative intensity as the salt concentration increases, which corresponds to a decrease in the sphere–wall separation distance. This trend is expected: the Debye length decreases as the ionic strength increases, which weakens double-layer repulsion and leads to a decrease in the most-probable separation distance. When the particle is closer to the reflecting interface, the intensity of the evanescent wave is greater and correspondingly the intensity of the scattered light is greater. At ionic strengths >3 mM, it was more difficult to obtain histograms of scattering intensity due to sticking of the particles to the glass slide.

The displacements in the frequency maximum for each scattering histogram can be compared to those expected based on the measured change in solution conductivities. The actual and predicted displacements resulting from a change in ionic strength (relative to 3 mM NaCl) are shown in table 2. The range of predicted displacements at each ionic strength corresponds to a range of assumed values for the surface potentials from 25 to ∞ mV (equal potentials of both the sphere and the plate surfaces). Note that the actual and predicted shifts compare very well. The discrepancy seen at 0 mM can be attributed to the weak scattering intensity being near the limit of detectability of the PMT and to the significance of the background scattering with respect to this weak intensity. Additionally, this discrepancy may be due to the greater uncertainty in calculating κ since the identity of the ions in the 0 mM solution is unknown (the background electrolyte was assumed to be NaCl). That agreement is generally seen between the experimental and predicted shifts confirms the exponential dependence of double-layer repulsion on Debye length.

Potential energy diagrams

Potential energy diagrams derived from the scattering histograms in figure 4 are shown in figure 5. Note that the experimental potential energy diagrams agree very well with those predicted from [22], with the exception of the 3.0 mM NaCl solution in the region $h - h_2 < 0$. The predicted potential energy diagrams were constructed based on the respective measured solution conductivities, from which the Debye lengths were calculated; consequently, no adjustable parameters were required. The small differences between the predicted and experimental minima are due to the differences between h_2 and h_m.

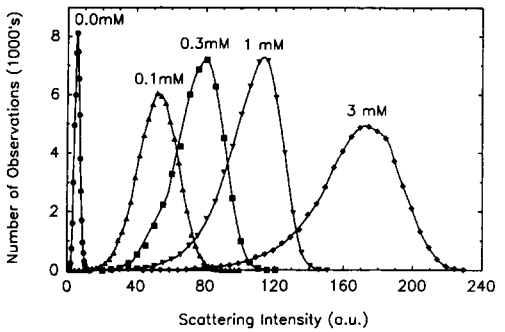

Figure 4. Histograms of scattering intensity for one 10 μm polystyrene latex sphere, each in solutions of different ionic strength.

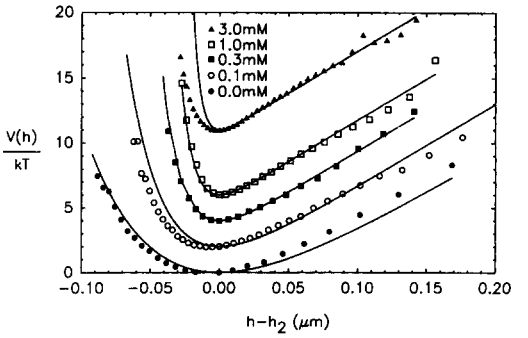

Figure 5. Potential energy diagrams for one 10 μm polystyrene latex sphere, each in a solution of different ionic strength from 0 to 3.0 mM NaCl corresponding to the histograms in figure 4.

Verification of TIRM to measure separation distances and thus colloidal forces is provided by the correspondence between the predicted and experimental profiles in the region $h - h_2 > 0$. In this region far from the glass slide, double-layer forces are negligible and only gravity acts on the sphere; the slope of the diagrams in this linear region represents the net weight of the sphere which can be easily calculated. This agreement also justifies the use of Chew *et al.*'s (1979) theory to analyze the scattering data.

TIRM has also demonstrated an ability to measure double-layer repulsion as shown by the agreement in the profiles for $h < h_2$ (with the exception of the 3.0 mM NaCl solution). In light of this agreement, the assumption of negligible van der Waals forces for the range of separation distances encountered at the lower strengths appears to be valid. It is expected that at higher ionic strengths, however, neither multiple reflections nor van der Waals forces can be neglected; in fact, attractive forces may account for the deviation of the experimental profile from the expected profile for the 3.0 mM solution in the region $h - h_2 < 0$.

Changing Incident Light Intensity

Of concern with the introduction of the higher-powered Ar ion laser was the presence of natural convection and radiation pressure, both of which would exert an extraneous force on the sphere. Natural convection is expected to result in movement of the particle that cannot be described by Brownian motion, and thus would lead to a discrepancy between the experimental and predicted profiles; this discrepancy would be more pronounced at higher laser intensities. Radiation pressure results from the elastic scattering of light by a particle (Askin 1970). The light incident on the particle transfers momentum to the particle, and through this transfer exerts a force which can cause acceleration of the particle. Radiation pressure in the TIRM experiments would give rise to a systematic movement of the particle due to momentum transfer from the evanescent wave, and this motion would be enhanced as the laser power was increased.

Using the Ar ion laser, the output power of the laser was changed at a constant wavelength of 514 nm (green light) to determine the importance of either effect in these experiments. Histograms of scattering intensity for one particle in a 1 mM NaCl solution at three different incident light intensities are shown in figure 6. The corresponding potential energy diagrams are shown in figure 7. Although the three potential energy diagrams are slightly different, no monotonic trend in the

Table 2. Comparison of the experimental and predicted shifts in the frequency maxima for the histograms in figure 4

			$h_2 - h_2$ at 3 mM (μm)	
mM NaCl	κ^{-1} (nm)	$I(h_2)$	Observed	Expected
0	55.6	9	0.30	0.36–0.50
0.1	22.8	52	0.12	0.13–0.17
0.3	15.4	81	0.08	0.08–0.11
1.0	9.57	115	0.04	0.03–0.05
3.0	5.56	174	0	0

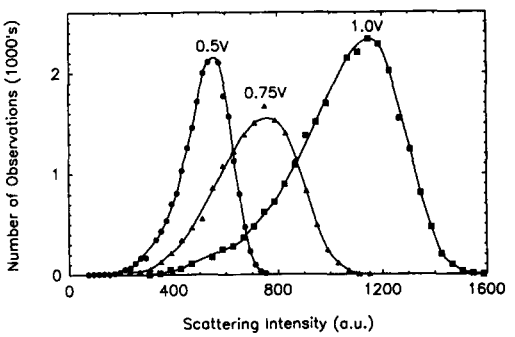

Figure 6. Histograms of scattering intensity for one 10 μm polystyrene latex sphere in 1.0 mM NaCl at three different light intensities.

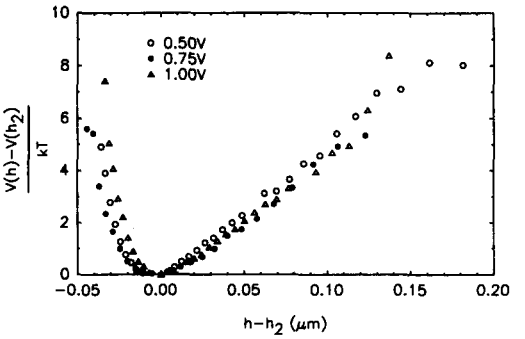

Figure 7. Potential energy diagrams for one 10 μm polystyrene latex sphere in 1.0 mM NaCl at three different incident light intensities corresponding to the histograms in figure 6.

differences with laser power is seen. For example, in the region $-0.04 \leqslant h - h_2 \leqslant 0.08$, the relative potential energy first decreases then increases with increasing laser power; outside of this range of separation distances, the change of potential energy with laser power is variable. The lack of a monotonic trend in the results with increasing laser power suggests that neither natural convection nor radiation pressure is important in these experiments.

From figure 7, the resolution of TIRM, which is given by the difference in separation distance between two adjacent data points, is better than 5 nm. This resolution is comparable to SEM. Unlike SEM, however, TIRM can be used to study dynamic processes in liquid media.

Measuring Absolute Separation Distances

As stated earlier, only relative separation distances can presently be measured with TIRM. In principle, the ability to measure absolute separation distances requires a knowledge of the intensity of the evanescent wave at the interface and the angles θ and ϕ over which the scattering cross section has been integrated by the PMT. One approach to measure absolute separation distances is to coat the glass slide with films of known thicknesses that are indexed-matched with the electrolyte solution, and then to adsorb the particle to the surface of the film. Measuring the scattering intensity as a function of film thickness for the adsorbed particles will yield a "calibration" curve, from which absolute separation distances can be obtained for nonadsorbed particles given the histogram of scattering intensities. By index-matching the film with the solution, we will avoid the problem of multiple reflections discussed previously. Part of our current research effort with TIRM is directed toward obtaining measurements of absolute separation distances.

INSIGHT FOR FUTURE EXPERIMENTS

The experimental results presented here demonstrate that TIRM provides the capability to observe the dynamic motion of a particle near a wall; consequently, TIRM can prove to be a powerful tool for measuring colloidal forces. TIRM has been used here to demonstrate the action of double-layer repulsion and gravity. One extension of this work is to measure van der Waals forces, which can be made significant by increasing the ionic strength of the solutions to diminish double-layer repulsion. One experimental difficulty with studying van der Waals forces may be sticking of the particles to the plate; however, careful selection of the sphere and plate materials can make these forces repulsive and thus alleviate such sticking. A second extension is to use TIRM to test experimentally Derjaguin's (1934) approximation for the particle size dependence of double-layer repulsion. While the limitations of Derjaguin's approximation have been investigated theoretically (e.g. Ring 1985; Barouch *et al.* 1986), a direct experimental test of this approximation has never been possible for single particle–single particle or single particle–substrate interactions. TIRM can now allow an experimental validation of the approximation for the single particle–substrate system. The main obstacle to achieving results at ionic strengths >10 mM will be overcoming the sticking of the particles to the glass slide.

Some anomalous behavior has been observed in the 0.1 and 10 mM solutions, which provides additional motivation for future studies. Shown in figure 8 are three consecutive scattering histograms (i.e. three consecutive 2-min sampling periods) for one particle in the 10 mM solution; the numbers above the histograms represent the order in which the data were obtained. A shifting of these histograms to higher relative intensity with increasing time is seen. Note that histogram 3 is narrow and nearly symmetric about the maximum; this suggests that the movement of the sphere was constrained to a small range of separation distances equally distributed about the most-probable separation distance. This behavior is indicative of reversible adsorption, and, if given enough time, the particle was often observed to exhibit a histogram similar to "1" or "2" after a "3" histogram. TIRM is well-suited to study such adsorption, and the technique can be applied to adsorption phenomena either in quiescent or moving fluids. As an extension, TIRM can be applied to the study of particle deposition onto or detachment from solid surfaces during flow. Additionally, TIRM can be used to study the phenomenon of electrokinetic lift (Bike 1988; Prieve & Bike 1987; Bike & Prieve 1990).

Shown in figure 9 are the scattering histograms for two particles in the same 0.1 mM NaCl dispersion. Particle 1 gives an "expected" histogram (see figure 4 for a comparison): i.e. the histogram is skewed toward lower intensities. However, a second particle ("2") in the same sample of the dispersion gives a narrow and nearly symmetric histogram. Although this is similar to histogram 3 in figure 8, it is not shifted to higher intensity; consequently, it is unlikely that the particle was adsorbed in a deeper potential energy well. One explanation for this observation is that the particle was held away from the slide by a semi-rigid tether. Such tethering would limit the range of separation distances that the particle could sample and would lead to a narrow histogram. van de Ven *et al.* (1983) have suggested that polystyrene latex particles possess "hairy" surfaces; these hairs could form the tethers holding the particle away from the slide. Note that tethering of particles can be readily studied by TIRM; one extension of this study is to characterize the steric interactions between a glass surface and a particle bearing adsorbed polymer layers. A second explanation for this observation is that the particle was held above the glass slide at a fixed position due to asperity contacts. Profiles of the slide surface obtained with phase detection interferometry have revealed asperities as large as 20 nm (Smryl 1989). It may be possible that surface roughness of the slide and/or the sphere resulted in such asperity contacts which have been detected as particle "sticking" and have hindered the use of this technique at ionic strengths >3 mM.

Additionally, TIRM can be used to study the dynamics of particle motion near a wall. These experiments would yield separately the diffusion coefficients of the particle in directions normal to and parallel to the wall; note that this decoupling of the coefficients was not possible using photon correlation spectroscopy with particle ensembles located in an evanescent wave (Lan *et al.* 1986). Also, TIRM can be used to study the behavior of biological particles near a wall. Preliminary attempts have been made to characterize the double-layer interactions between a red blood cell and a glass slide using TIRM (Pino 1988).

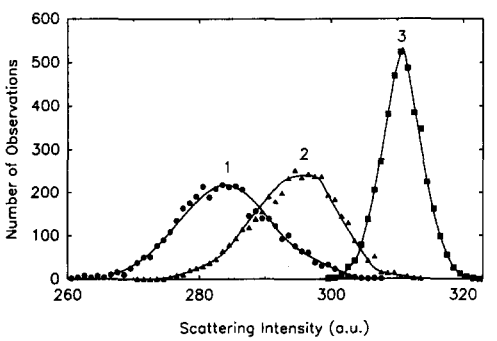

Figure 8. Scattering histograms at 2-min intervals for one 10 μm polystyrene latex sphere in 10 mM NaCl; evidence of reversible adsorption. Histogram 1 corresponds to sampling during the 0–2 min time interval; histogram 2 corresponds to sampling during the 2–4 min time interval; and histogram 3 corresponds to sampling during the 4–6 min time interval.

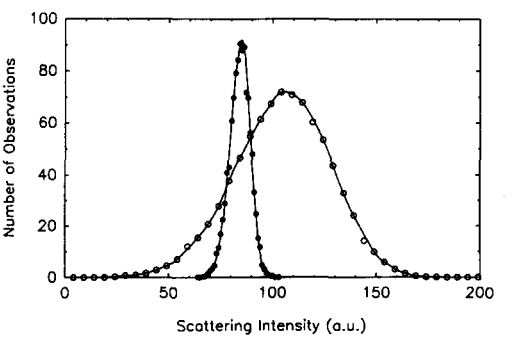

Figure 9. Scattering histograms for two different particles in 0.1 mM NaCl: evidence of tethering. Particle 1 appears to be mobile, while particle 2 appears to be tethered.

CONCLUSIONS

TIRM provides the capability to observe noninvasively dynamic particle motion near a wall in liquid media. The spatial resolution of TIRM is comparable to SEM. Potential energy diagrams for a polystyrene microsphere interacting with a glass plate in electrolyte solutions were obtained which demonstrated the action of double-layer and gravity forces. In addition, these experimental diagrams compared well with those predicted from models of double-layer and gravity forces which involved no adjustable parameters. That the most-probable intensity of scattered light increased with ionic strength, as predicted by the double-layer force model, was quantitative confirmation of that model. More importantly, the slope of the potential energy diagrams in the region where gravity was the dominant force agreed well with the known force of gravity; this agreement provided the strongest confirmation of the TIRM technique as a quantitative tool for the study of surface forces. Future applications of TIRM include measuring van der Waals and steric forces, and evaluating the particle-size dependence of double-layer repulsion with respect to Derjaguin's approximation.

Acknowledgements—This work was supported by the National Science Foundation. We thank Professor W. H. Smyrl of the University of Minnesota for the surface profiles.

REFERENCES

ALEXANDER, B. M. & PRIEVE, D. C. 1987 A hydrodynamic technique for measurement of colloidal forces. *Langmuir* **3,** 788–795.

ALLAIN, C., AUSSERRE, D. & RONDELEZ, F. 1982 Direct optical observation of interfacial depletion layers in polymer solutions. *Phys. Rev. Lett.* **49,** 1694–1697.

ASHKIN, A. 1970 Acceleration and trapping of particles by radiation pressure. *Phys. Rev. Lett.* **24,** 156–159.

AUSSERRE, D., HERVET, H. & RONDELEZ, F. 1985 Concentration profile of polymer solutions near a solid wall. *Phys. Rev. Lett.* **54,** 1948–1951.

AXELROD, D., BURGHARDT, T. P. & THOMPSON, N. L. 1984 Total internal reflection fluorescence. *A. Rev. Biophys. Bioengng* **13,** 247–268.

BAROUCH, E., MATIJEVIC, E. & PARSEGIAN, V. A. 1986 The accuracy of the Derjaguin approximation for the electrostatic double-layer interaction between curved surfaces bearing constant potentials. *J. chem. Soc. Faraday Trans. I* **82,** 2801–2809.

BEISSINGER, R. L. & LEONARD, E. F. 1980 Immunoglobulin sorption and desorption rates on quartz: evidence for multiple sorbed states. *Am. Soc. artif. intern. Organs J.* **3,** 160–175.

BIKE, S. G. 1988 Electrokinetic lift. Ph.D. Thesis, Carnegie Mellon Univ., Pittsburgh, Pa.

BIKE, S. G. & PRIEVE, D. C. 1990 Electrohydrodynamic lubrication with thin double layers. *J. Colloid Interface Sci.* In press.

CHEW, H., WANG, D.-S. & KERKER, M. 1979 Elastic scattering of evanescent electromagnetic waves. *Appl. Opt.* **18,** 2679–2687.

CHRISTENSON, H. K. 1984. DLVO (Derjaguin–Landau–Verway–Overbeek) theory and solvation forces between mica surfaces in polar and hydrogen-bonding liquids. *J. chem. Soc. Faraday Trans. I* **80,** 1933–1946.

CHRISTENSON, H. K. & HORN, R. G. 1983 Direct measurement of the force between solid surfaces in a polar liquid. *Chem. Phys. Lett.* **98,** 45–48.

CHRISTENSON, H. K., HORN, R. G. & ISRAELACHVILI, J. N. 1982 Measurement of forces due to structure in hydrocarbon liquids. *J. Colloid Interface Sci.* **88,** 79–88.

DERJAGUIN, B. V. 1934 Friction and adhesion IV. The theory of adhesion of small particles. *Kolloid-Z.* **69,** 155–164.

ISRAELACHVILI, J. N. 1978 Measurement of forces between surfaces immersed in electrolyte solutions. *Faraday Discuss. chem. Soc.* **65,** 20–24.

ISRAELACHVILI, J. N. & ADAMS, G. E. 1976 Direct measurement of long-range forces between two mica surfaces in aqueous KNO_3 solutions. *Nature* **262,** 774–776.

ISRAELACHVILI, J. N. & ADAMS, G. E. 1978 Measurement of forces between two mica surfaces in aqueous electrolyte solutions in the range 0–100 nm. *J. chem. Soc. Faraday Trans. I* **74,** 975–1001.

ISRAELACHVILI, J. N., TANDON, R. K. & WHITE, L. R. 1980 Measurement of forces between two mica surfaces in aqueous polyethylene oxide solutions. *J. Colloid Interface Sci.* **78,** 430–443.

ISRAELACHVILI, J. N., TANDON, R. K. & WHITE, L. R. 1984 Forces between two layers of adsorbed polystyrene immersed in cyclohexane below and above the θ temperature. *Macromolecules* **17,** 204–209.

LAN, K. H., OSTROWSKY, N. & SORNETTE, D. 1986 Brownian dynamics close to a wall studied by photon correlation spectroscopy from an evanescent wave. *Phys. Rev. Lett.* **57,** 17–20.

LANNI, F., WAGGONER, A. S. & TAYLOR, D. L. 1985 Structural organization of interphase 3T3 fibroblasts studied by total internal fluorescence microscopy. *J. Cell Biol.* **100,** 1091–1102.

LIPSON, S. G. & LIPSON, H. 1981 *Optical Physics.* Cambridge Univ. Press, New York.

PINO, M. A. 1988 The use of total internal reflection microscopy to examine colloidal forces. Master's Thesis, Carnegie Mellon Univ., Pittsburgh, Pa.

PRIEVE, D. C. & ALEXANDER, B. M. 1986 Hydrodynamic measurement of double-layer repulsion between colloidal particles and a flat plate. *Science* **241,** 1269–1270.

PRIEVE, D. C. & BIKE, S. G. 1987 Electrokinetic repulsion between two charged bodies undergoing sliding motion. *Chem. Engng Commun.* **55,** 149–164.

PRIEVE, D. C., LANNI, F. & LUO, F. 1987 Brownian motion of a hydrosol particle in a colloidal force field. *Faraday Discuss. chem. Soc.* **83,** 297–307.

RABINOWICH, VA. I., DERJAGUIN, B. V. & CHURAEV, N. V. 1982 Direct measurement of long-range surface forces in gas and liquid media. *Adv. Colloid Interface Sci.* **16,** 63–78.

RING, T. A. 1985 Upper-bound error estimates for the Derjaguin approximation and the linearization approximation to the double-layer interaction energy for two unequal spheres. *J. chem. Soc. Faraday Trans. II* **81,** 1193–1200.

SMRYL, W. H. 1989 Unpublished data.

TEMPLE, P. A. 1981 Total internal reflection microscopy: a surface inspection technique. *Appl. Opt.* **20,** 2656–2664.

VAN DE VEN, T. G., DABROS, T. & CZARNECKI, J. 1983 Flexible bonds between latex particles and solid surfaces. *J. Colloid Interface Sci.* **93,** 580–581.

WATKINS, R. W. & ROBERTSON, C. R. 1977 A total internal reflection technique for the examination of protein adsorption. *J. biomed. Mater. Res.* **11,** 915–938.